Electronic Supplementary Material (ESI) for Soft Matter.

Supporting Information

Compression of colloidal monolayers at liquid interfaces: *in situ vs. ex situ* investigation

Keumkyung Kuk,[a] Vahan Abgarjan,[a] Lukas Gregel,[a] Yichu Zhou,[a] Virginia Carrasco Fadanelli,[b] Ivo Buttinoni,[b] and Matthias Karg[a]*

[a]Institut für Physikalische Chemie I: Kolloide und Nanooptik, Heinrich-Heine-Universität Düsseldorf, Universitätsstr. 1, 40225 Düsseldorf, Germany

[b]Institut für Experimentelle Physik der kondensierten Materie, Heinrich-Heine-Universität Düsseldorf, Universitätsstr. 1, 40225 Düsseldorf, Germany

***In situ* fluorescence microscopy of the main CS microgel at low Π**

Figure S1 shows a microscopy image (*in situ*) of a monolayer of the main CS microgel (the same CS microgel presented in **Figure 1-4** – the main CS microgel). Here, Π is very low (0.2 mM/m) but still showing that attractive interactions are present at the interface.

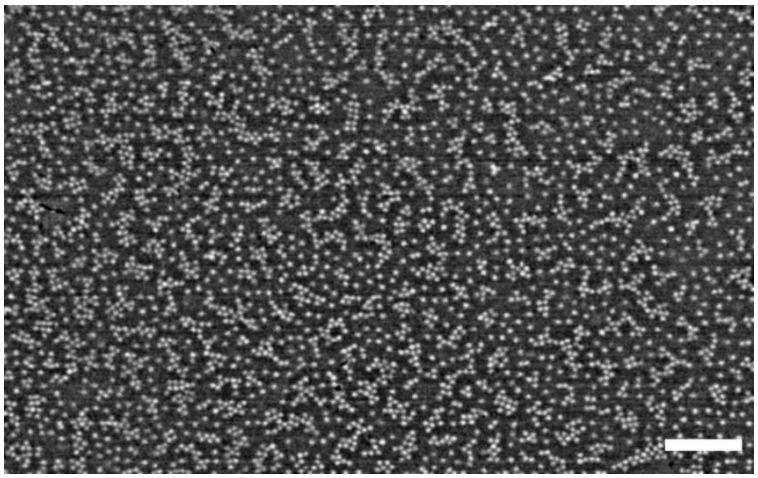

Figure S1. Fluorescence microscopy image (**Method2**) of a CS microgel monolayer at Π = 0.2 mM/m. The scale bar corresponds to 20 μm. The image was processed by ImageJ (Bandpass filter – Gaussian Blur) for better visibility.

Additional *ex situ* vs. *in situ* differences for the main CS microgels

Figure S2A shows $D_{c\text{-}c}$ plotted as a function of the particle number per unit area (n_P/A). Theoretical values of $D_{c\text{-}c}$ for close-packed, perfectly hexagonally ordered monolayers were calculated according to our already published work.[1] These values are compared with *ex* and *in situ* microscopy data. **Figure S2B** illustrates the systematic shift of n_P/A in *ex situ* measurement compared (filled squares) to the *in situ* method (open squares) at the same measured Π.

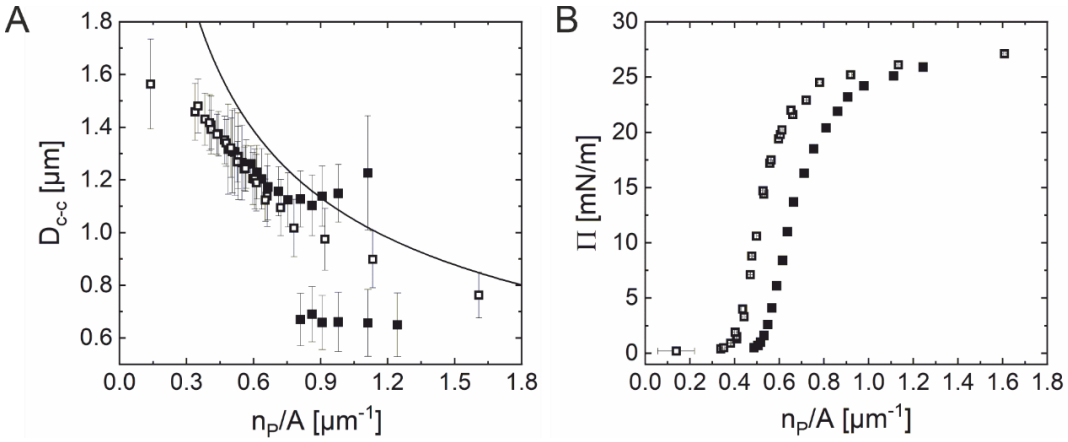

Figure S2. A) $D_{c\text{-}c}$ as a function of n_P/A. The solid line corresponds to the calculated, theoretical evolution of $D_{c\text{-}c}$ (under the assumptions that the monolayer has a perfect hexagonal symmetry with the area fraction of 0.9069). The filled squares correspond to the *ex situ* and the empty squares to the *in situ* measurement results, respectively. B) Π as a function of n_P/A obtained from *ex situ* (filled squares) and *in situ* (empty squares) measurements.

Monolayers of silica particles

The monolayer of silica particles shown in **Figure 7A** of the main manuscript was transferred and dried onto a solid substrate using Langmuir-Blodgett deposition. **Figure S3** shows microscopic images and SALS patterns of these monolayers for different values of Π (see caption). The diffraction patterns vary from ring-like to peak-like depending on the position on the substrate.

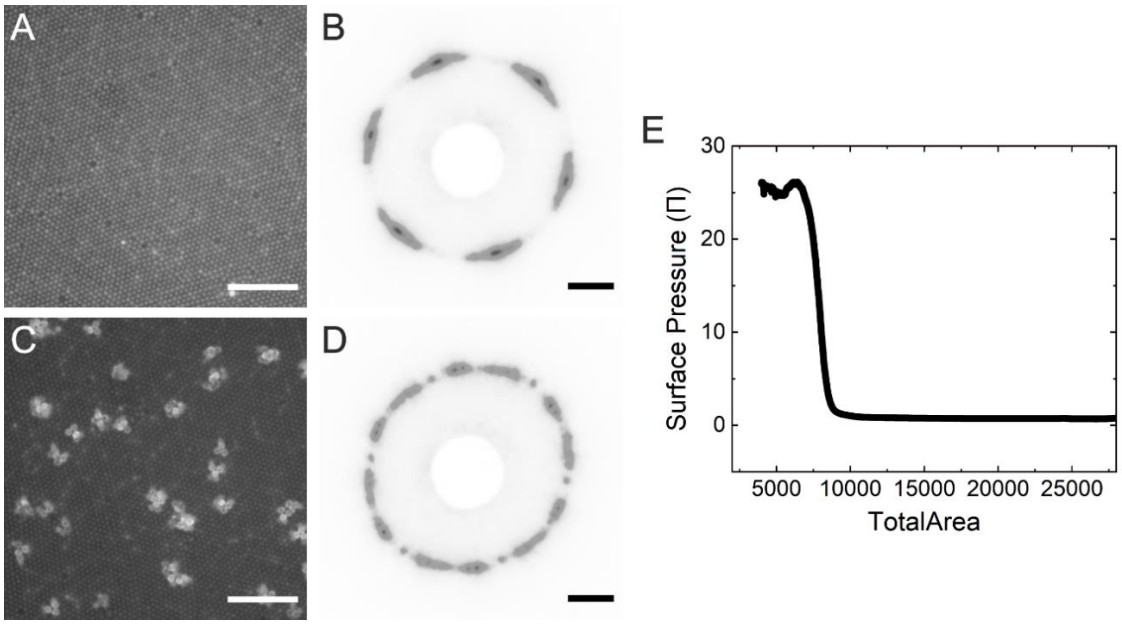

Figure S3. A) Optical light microscopy image and B) diffraction pattern of a dried silica monolayer (*ex situ*) at Π = 0.5 mN/m. C) and D) show the same but at Π of approximately 20 mN/m. The scale bars in A) and C) correspond to 10 μm. The scale bars in B) and D) correspond to 10 mm. E) Compression isotherm recorded during the Langmuir-Blodgett deposition.

Monolayers of (coreless) PNIPAM microgels

The system of coreless microgels shown in **Figure 7B** of the main manuscript was also investigated *in situ* using fluorescence microscopy (**Method 2**), also in a range of values of Π where the interparticle distance is too large to be resolved in our current LT-SALS setup. **Figure S4** shows microscopic images of the microgel monolayer at different Π. We do not observe an "isostructural phase transition".

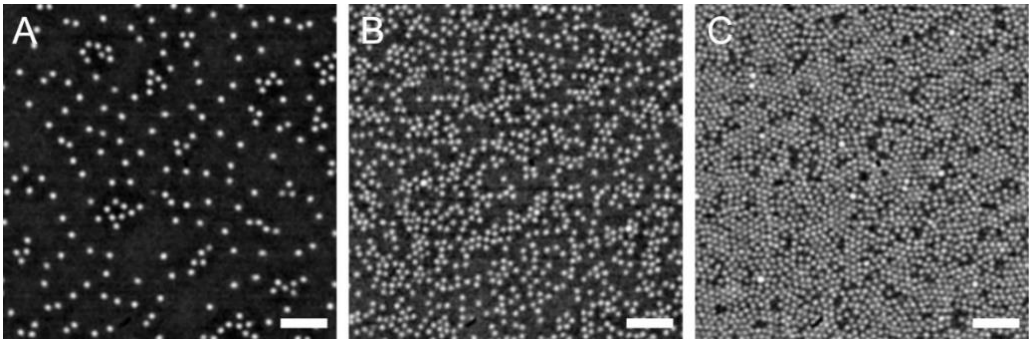

Figure S4. Microgel monolayer (*in situ*) for A) Π = 3.7, B) Π = 28.4, and C) Π = 29.2 mN/m. The scale bars correspond to 10 μm. The images were processed by ImageJ (Bandpass filter – Gaussian Blur) for better visibility.

The same monolayer of microgels was then studied *ex situ* after Langmuir-Blodgett deposition. **Figure S5A** and **C** show optical light microscopy images of the dried microgel monolayers prepared at two different Π of 30.2 (black) and 31.2 mN/m (red). **Figure S5B** and **D** show AFM images of the corresponding microgel monolayers. **Figure S5E** shows calculated radial distribution functions (RDFs) as well as nearest neighbor center-to-center distances, $D_{c\text{-}c}$. **Figure S5F** displays the diffraction pattern recorded by SALS, representative for the microgel monolayers taken from Π between 30.2 and 31.2 mN/m.

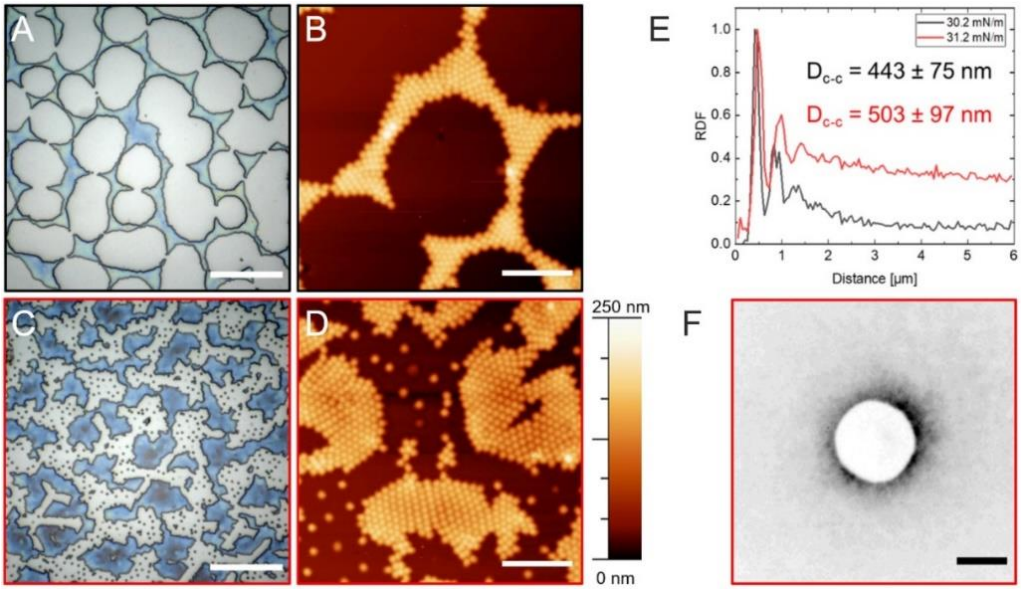

Figure S5. A) Microgel monolayer (*ex situ*) at Π = 30.2 mN/m observed by light microscopy. The scale bar corresponds to 20 µm. B) Observation by AFM. The scale bar corresponds to 5 µm. C)-D) The same data set for the microgel monolayer (*ex situ*) at Π = 31.2 mN/m. E) Interparticle distance analysis from RDF. F) Scattering pattern of the microgel monolayer from C). The scale bar corresponds to 10 mm.

AFM images of CS microgel from Figure 9 – 105 nm (4.8)

The microscopic image of CS microgel (D_c = 105 nm, shell-to-core size ratio: 4.8) in **Figure 9C2** (dried in open air) of the main manuscript could not be resolved due to the relatively homogeneous refractive index of the microgel, in comparison with **Figure 9C1** (dried with heat gun). **Figure S6A** and **C** show AFM measurements on these monolayers at lower Π (10 mN/m), and **Figure S6C** and **D** are the corresponding phase images.

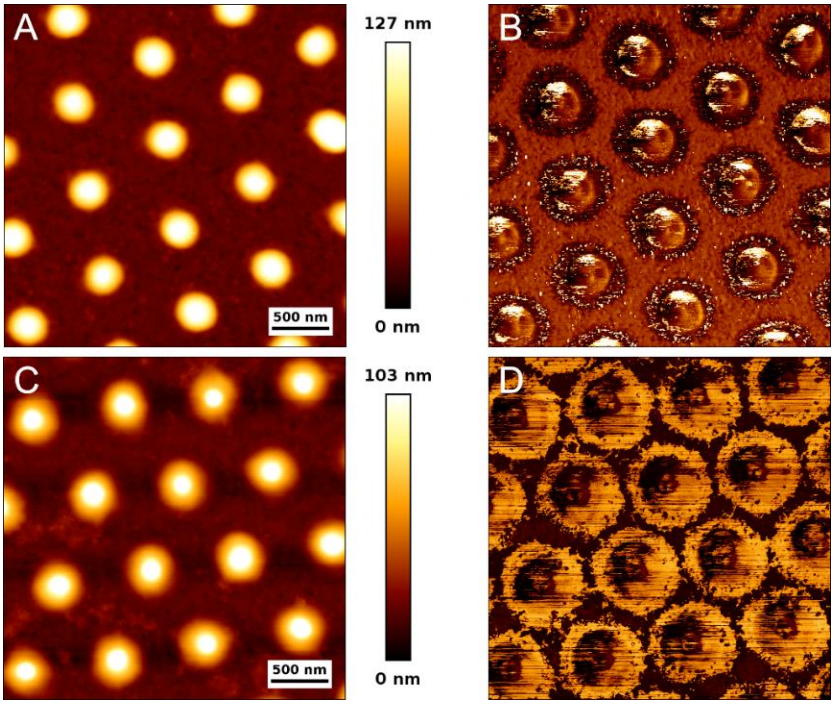

Figure S6. A) AFM image of CS microgel – 105 nm (4.8) – monolayer dried with heat gun. B) Corresponding phase image of A). C)-D) The same set of data for the monolayer dried in open air at room temperature.

Interparticle distance from LT-SALS

The interparticle distance measured by LT-SALS (D_{c-c}^{SALS}) was calculated as below:

$$q = \frac{4\pi n}{\lambda} \sin\left(\frac{1}{2} atan\left(\frac{xy}{D_{S-D}}\right)\right)$$

where q is the magnitude of the scattering vector in μm^{-1}, n the refractive index (refractive index of air, n = 1), λ the wavelength of the light in μm, x the distance from primary beam in pixel, y the conversion factor in mm per pixel and $D_{S\text{-}D}$ the sample-to-detector distance in mm. The scattering vector yields the lattice spacing $D_{hk} = \frac{2\pi}{q}$. For a two-dimensional, hexagonally ordered system, the interparticle distance is $D_{c-c} = \frac{2}{\sqrt{3}} d_{hk}$. With a blue diode laser (λ = 405 nm), the available q-

value ranges from 0.39 to 15.74 µm^{-1} ($D_{c\text{-}c}$ approximately from 460 nm up to 18 µm). With a green and red diode laser (λ = 532 nm, 632.8 nm), the available q-value ranges from 0.30 to 11.98 µm^{-1} ($D_{c\text{-}c}$ approximately from 600 nm up to 24 µm) and from 0.25 to 10.07 µm^{-1} ($D_{c\text{-}c}$ approximately from 720 nm up to 29 µm), respectively. **Figure S7** depicts LT-SALS measurements done with blue and red lasers as well as the $D_{c\text{-}c}$ range for three different laser types graphically.

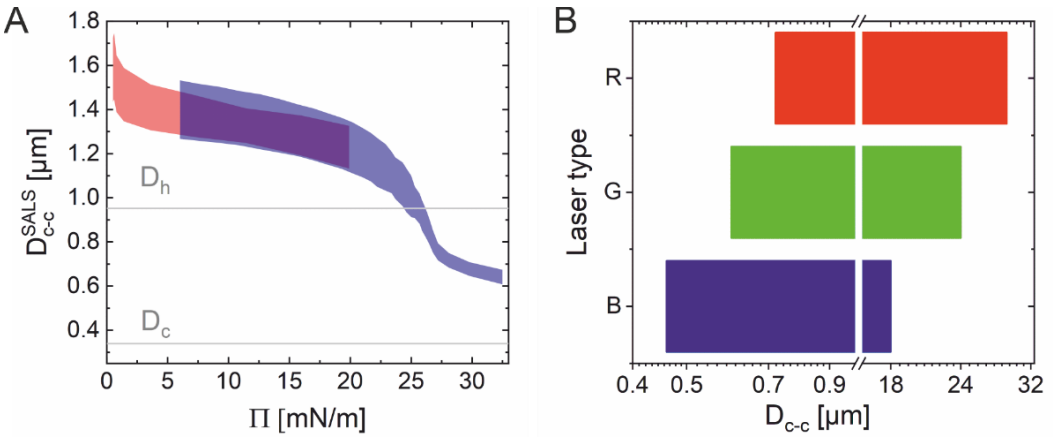

Figure S7. A) LT-SALS measurement done with blue and red lasers on the same CS microgel. B) Calculated possible range of $D_{c\text{-}c}$ for different laser wavelengths for our setup, R-red, G-green and B-blue.

Image processing and analysis by ImageJ (1.53k, National Institutes of Health, USA)

Radial Distribution Functions (RDFs) were calculated with ImageJ macro version 2011-08-22 by Ajay Gopal using the center of mass positions of each CS microgel. To find the centers, the *ex situ* light microscopy images were pre-processed with Gaussian blur. Particles at the edges of the images were excluded. The *in situ* fluorescence microscopy images were then processed with Bandpass filter, background subtraction and Gaussian blur. Grey scaled LT-SALS images were radially and azimuthally averaged by Radial Profile Plot (Version 2009-08-14 by Paul Baggethun) and Azimuthal Average (Version 2007-09-08 by Philippe Carl), respectively.

LT-SALS setup

The level of accuracy was checked with all the involved components in the laser path using a circular level. The laser was aligned with the camera center with two mirrors and through the microscopy window of the trough by using a pinhole on a rail, which consisted of two parallel rods screwed into the optical plate. After the alignment, the rail and the pinhole were removed. The Langmuir trough and the camera were placed back in the laser path. The paper screen (width: 90 mm) was rolled around two metal rods, fastened parallel to the trough and fixed on the customized frame, see **Figure S8**. The laser beam center was marked on the screen for various size of beam stops to be glued on when required. The sample-to-detector distance ($D_{S\text{-}D}$) was measured with a ruler ensuring all four corners of the screen have the same distance to the trough wall. The pixel/mm value was determined using millimeter paper after all the involved components were fixed on their positions. The screen was rolled back and put aside on one metal rod for the cleaning of the trough. The trough was filled again with water before the screen was rolled out and fixed back to its position. Then the monolayer was deposited at the air/water interface. The $D_{S\text{-}D}$ of our current setup could be varied from 25 to 200 mm (scattering angle ranges from 2 - 74°).

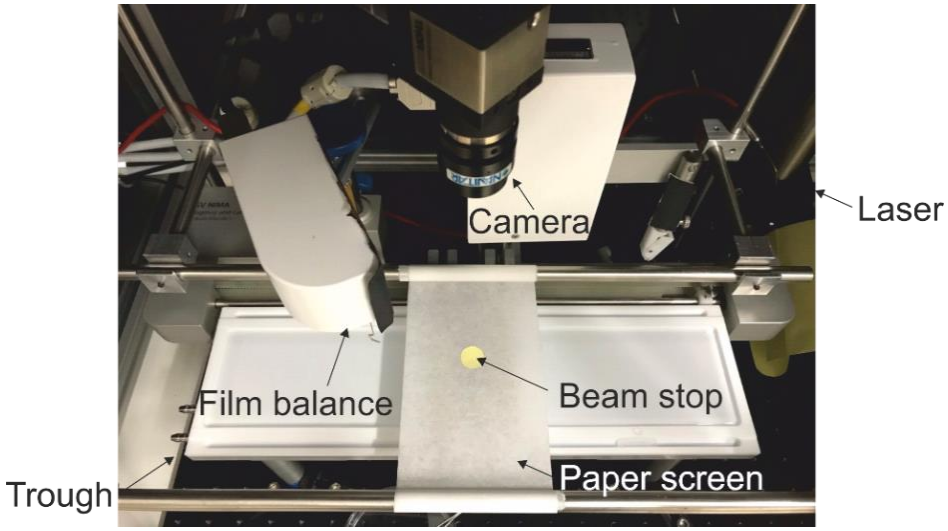

Figure S8. Photograph of the LT-SALS setup.

REFERENCES

1. K. Kuk, L. Gregel, V. Abgarjan, C. Croonenbrock, S. Hänsch and M. Karg, *Gels*, 2022, **8**, 516.